Journal of Power Sources 195 (2010) 1195–1201

Contents lists available at ScienceDirect

Journal of Power Sources

journal homepage: www.elsevier.com/locate/jpowsour

Structural and transport evolution in the $Li_xAg_2V_4O_{11}$ system

F. Sauvage [a], V. Bodenez [b], H. Vezin [c], M. Morcrette [b], J.-M. Tarascon [b], K.R. Poeppelmeier [a,*]

[a] Department of Chemistry and Materials Research Center, Northwestern University, 2145 Sheridan Rd., Evanston, IL 60208-3113, USA
[b] LRCS, UMR CNRS 6007, Université de Picardie Jules Verne, 33 rue St.-Leu, 80039 Amiens Cedex, France
[c] LCOM, CNRS UMR 8009, Bat. C4, 59655 Villeneuve d'Ascq Cedex, France

ARTICLE INFO

Article history:
Received 10 July 2009
Received in revised form 28 August 2009
Accepted 31 August 2009
Available online 4 September 2009

Keywords:
Primary lithium batteries
ICD
Cathode
SVO
$Ag_2V_4O_{11}$
In situ XRD measurements

ABSTRACT

We investigated the effect of inserting lithium into $Ag_2V_4O_{11}$ (ε-SVO) on the structure, electronic properties and redox committed by combining *in situ* XRD measurements, ESR spectroscopy and 4 probes DC conductivity coupled with thermopower measurements. The electrochemical discharge occurs in three consecutive steps above 2 V (vs. Li^+/Li). The first one, between $0 < x < \sim 0.7$ in Li_x-SVO, has been ascribed to the V^{5+} reduction through a solid solution mechanism. This reduction competes with a Li^+/Ag^+ displacement reaction which leads to a structural collapse owing to the ionic radii mismatch between the withdrawn Ag^+ and the inserted Li^+. The silver reduction progresses continuously with two different slopes along two composition–potential plateaus at 2.81 V and 2.55 V. Finally, the reduction continues until we obtain an amorphous structure with V^{4+} and a ε of V^{3+}. Although, the silver re-enters the structure during the subsequent recharge, the original structure is not recovered. The reduction of silver forming silver metal nano-clusters acts to increase the electronic conductivity from 3.8×10^{-5} S cm^{-1} to 1.4×10^{-3} S cm^{-1}. In complement to this study, we also report on a low temperature hydro-(solvo)-thermal approach using $HF_{(aq)}$ as a mineralizer, which enables the synthesis of nano-sized ε-SVO particles that exhibit superior electrochemical performances compared to conventional particles synthesized by solid-state reaction.

1. Introduction

The combination of high chemical/electrochemical stability [1] and good electron/ion transport in the solid ($\sigma_{e^-} \sim 10^{-2}$ to 10^{-3} S cm^{-1} and $D_{(Li^+)} \sim 10^{-8}$ cm^2 s^{-1}) [2–5] has enabled the introduction of $Ag_2V_4O_{11}$ (ε-SVO) as cathode for high rate primary lithium batteries in Implantable Cardioverter Defibrillators (ICD). This medical appliance, essentially devoted to pace and sense heart functions as well as to treat ventricular fibrillation, provides a shock to the right ventricle with an energy that can be as high as 25–40 J. Research in ε-SVO has concentrated on optimizing the electrochemical performance vs. lithium; this was done by adjusting the synthetic route [6–9] or by modifying the ε-SVO/electrolyte interface to enhance charge transfer efficiency [5,10].

From a fundamental standpoint, the mechanism of lithium insertion is particularly complex due to a multiple-step process involving the reaction of approximately 6 Li^+ at a cut-off potential of 2 V [11]. *Ex situ* X-ray powder diffraction on different lithiated ε-SVO has identified (i) a Li^+/Ag^+ displacement reaction [3,12,13], (ii) the reduced silver morphology investigated by transmission or scanning electron microscopy [4,14] and (iii) Li, V and Ag local environment probed by nuclear magnetic resonance and X-ray absorption spectroscopies [15]. In complement to these studies, *in situ* X-ray diffraction measurements during lithium insertion/de-insertion and electron spin resonance (ESR) spectroscopy to investigate the V^{5+} reduction were combined with conductivity and thermopower measurements as a function of lithium composition to better understand the Li_x-SVO system, and thereby to provide more insight into the relationship between the state of discharge, electrode structure and the transport properties. In complement to such a fundamental study, we also report on reactivity enhancement using flat needle-like particles that have been prepared by a hydro(-solvo-) thermal route using $HF_{(aq)}$ as a mineralizer.

2. Experimental

2.1. ε-SVO synthesis procedures

$Ag_2V_4O_{11}$ was successfully synthesized as a single phase either by solid-state reaction (SVO-SSR) or under hydrothermal conditions (SVO-HT). The first sample was made by forming a pellet containing a stoichiometric mixture of Ag_2O and V_2O_5 prior to heat treatment at 525 °C under air during 12 h. These particles were

* Corresponding author. Tel.: +1 847 491 3505.
E-mail address: krp@northwestern.edu (K.R. Poeppelmeier).

0378-7753/$ – see front matter © 2009 Elsevier B.V. All rights reserved.
doi:10.1016/j.jpowsour.2009.08.091

used for the *in situ* XRD measurements because of their higher crystallinity.

SVO-HT was prepared following a hydro(-solvo-)thermal approach and $HF_{(aq)}$ used as a mineralizer (Aldrich, 48–50% by weight). The originality of this synthesis lies in the use of semi-permeable FEP-Teflon pouches which contained the reacting media and particularly the $HF_{(aq)}$. Weights of $m(Ag_2O) = 0.2678$ g, $m(V_2O_5) = 0.5252$ g and $m(HF_{(aq)}) = 0.832$ g were introduced into the FEP-Teflon pouch, which correspond to a $Ag/V/HF_{(aq)}$ molar ratio of 1/2.5/35. The pouches, up to six, were placed in a 125 mL PTFE Teflon-lined autoclave (Parr Instruments) and backfilled with 42 mL de-ionized H_2O. The autoclave was then heated during 24 h at 150 °C and gradually cooled down to room temperature at 0.1 °C min^{-1}. A water uptake of around 0.30 g per pouch occurred as a result of the FEP-Teflon semi-permeability to water above 120 °C. The reaction completed, the pouches were carefully opened under air and the brown product retrieved by vacuum filtration in 60% yield based on the Ag content.

2.2. Physical characterization

XRD analysis of the pristine particles and *in situ* experiments were carried out in a $(\theta/2\theta)$ configuration using a Bruker D8 diffractometer. A homemade cell, similar to a Swagelok cell with the top capped by a beryllium window, was specifically designed to enable *in situ* observations. A Mac Pile galvanostat system controlled the cell discharge/charge. ESR experiments were carried out at room temperature with a Bruker ELEXYS E580 spectrometer. The particle size and morphology were determined using an Environmental Scanning Electron Microscope (ESEM) FEI Quanta 200FEG coupled with an Energy Dispersion Spectroscopy analysis system (EDS—Oxford Link Isis). The chemical reduction of SVO-HT particles was conducted in a N_2-filled dry box. To do this, an appropriate amount of LiI was dissolved in 25 mL anhydrous CH_3CN (Aldrich, 98%). This slurry was maintained under stirring 5 days at room temperature to complete the chemical-driven reduction. The transport measurements were performed on variously reduced Li_xSVO-HT pellets displaying ~80% compactness. Using a uni-axial press, the pellets were shaped by gradually compacting to 4 ton cm^{-2} the particles, and maintained at this pressure for at least 30 min. Room temperature DC conductivity was measured by a standard 4-probe Pt device (Cascade Microtech, Beaverton, OR). The error bar was defined by repeating the measurements at least five times among different pellet locations. Correction from porosity was taken into consideration by applying the Bruggeman symmetric medium equation (see below) assuming continuous interconnected porosity as described by McLachlan et al. [16]:

$$\sigma_{experimental} = \sigma_{real}\left(1 - \frac{3}{2}f\right)$$

where f represents the volume fraction of porosity. Room temperature thermopower measurements were performed by sandwiching the pellet between a heat source and a cold sink with gold foil electrodes and welded thermocouples. Thermovoltages ΔV and temperature gradient ΔT were monitored during the decay of a short heat pulse to 100 °C, from which the Seebeck coefficient was extracted (for $\Delta T < 20$ K) after correction from the thermopower contribution of the platinum. Assuming small polaronic-type conduction in the Li_x-SVO system, the thermopower values were converted to charge carrier concentration using the follow formalism [17,18]:

$$Q = -\frac{k_B}{e}\ln\left(\frac{\beta(1-c)}{c} + \frac{S_T^*}{k_B}\right)$$

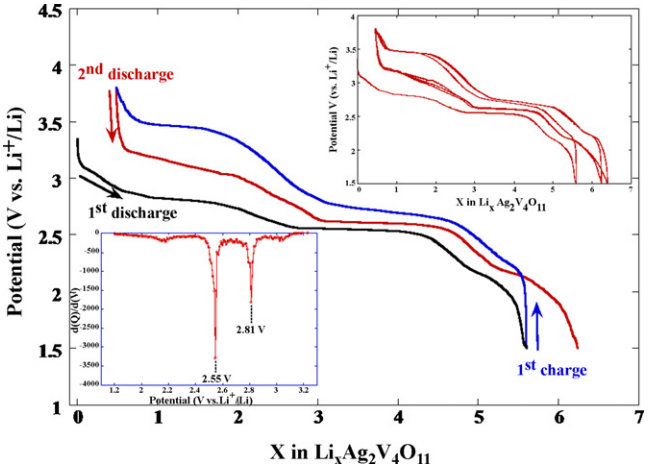

Fig. 1. Galvanostatic curve of the lithium insertion in $Ag_2V_4O_{11}$ and reversibility of the process from $Li_{5.6}$-SVO with subsequent lithium insertion curve (the three first cycles and derivative curve corresponding to the first discharge are shown in inset).

where k_B is Boltzmann's constant, e the electron charge; the spin degeneracy factor (β) is kept at 2, S_T^* represents the vibrational entropy associated with the ions surrounding a polaron in a given site, and c is the fraction of sites occupied by electrons, so that the electron concentration is given by $c{\cdot}N$, where N stands for the concentration of atomic sites (*i.e.* the V-site density in $Ag_2V_4O_{11}$ is 1.927×10^{22} cm^{-3}). The term S_T^*/k was herein neglected as it contributes to less than 10 μV K^{-1} to Q [17].

2.3. Electrochemical tests

The electrochemical characterization of the particles was carried out by thoroughly mixing the active material with 14% by wt. of sp-type carbon black (C_{sp}). The measurements were recorded using a two-electrode Swagelok cell assembled in an Ar-filled glove box. A lithium metal foil was used both as counter and reference electrode. Two separator pieces of Whatman GF/D borosilicate glass fiber were soaked with 1 M $LiPF_6$ EC/DMC 1:1 electrolyte (LP30—Merck Selectipur grade). The Swagelok cells were monitored by a VMP multi-potentiostat (Biologic SA, Claix, France).

3. Results and discussion

3.1. Insertion/de-insertion mechanism in SVO

The insertion of lithium in SVO proceeds according to two main potential–composition plateaus at 2.81 V and 2.55 V (vs. Li^+/Li^0). This leads to the insertion of 6 Li^+ per formula unit (Fig. 1). These processes are found to be mostly reversible for the first cycles. However, there was a potential difference between the first discharge and the subsequent ones, which noticeably affects the potential of the first plateau at 2.81 V.

The primary technique used in this survey was *in situ* XRD to scrutinize the processes occurring during the insertion/de-insertion of lithium as well as to better define the origin of the anodic potential shift. For this, the cathode reduction/oxidation was maintained at C/10 rate to accurately monitor the structural modification. XRD patterns were collected each $x = 0.11$ Li^+ inserted. In Fig. 2a, we plotted the diffractograms recorded between $x = 0$ and $x = 2$ in $Li_xAg_2V_4O_{11}$ (Li_xSVO). In this portion of the discharge, two main features are highlighted. The first one, taking place in the earlier step of insertion, occurs as a solid solution-type lithium insertion as shown by the progressive shift of the (−4 0 2) and (0 0 2) diffraction peaks (Fig. 2a). The inserted lithium occupies

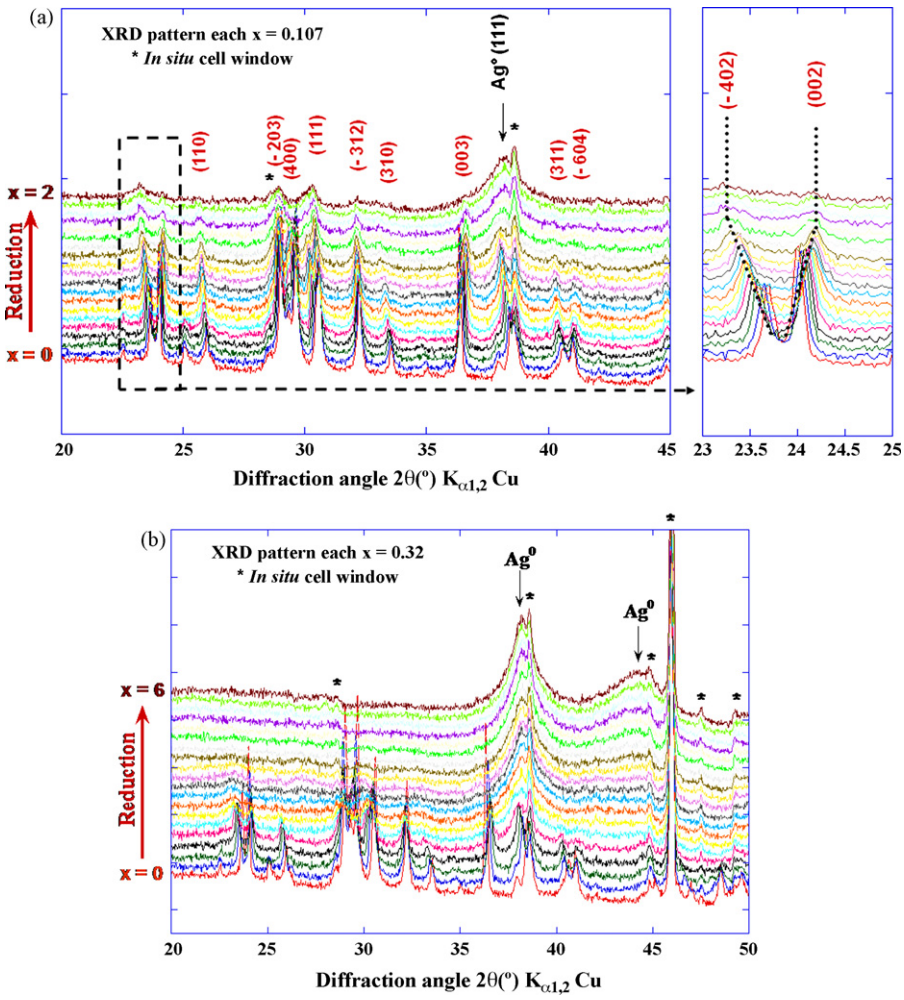

Fig. 2. *In situ* evolution of the XRD pattern recorded at a D/10 discharge rate: (a) every 0.107 Li^+ inserted between Li_0-SVO and Li_2-SVO and (b) every 0.32 Li^+ inserted between Li_0-SVO and Li_6-SVO.

available interstitial positions in the structure associated with the reduction of V^{5+} into V^{4+}. The presence of V^{4+} species has been observed by ESR with the feature of a broad signal at $g = 1.96$ assigned to the onset of paramagnetic V^{4+} on a sample electrochemically discharged to $x = 0.3$ Li^+. The second characteristic, initiated at $x \approx 1$, highlights the emergence of two broad diffraction peaks at $2\theta = 38.2^\circ$ and 44.2° ascribed to the (1 1 1) and (2 0 0) reflections of silver metal. This confirms the silver displacement reaction by lithium ions (Fig. 2b). Because of the structural strains occurring during this displacement reaction, the $Ag_2V_4O_{11}$ structure collapses due to the significant ionic radii mismatch between silver and lithium ions ($r_{(Ag+)} = 1.15$ Å and $r_{(Li+)} = 0.76$ Å [19]). This demonstrates a lack of flexibility between the V_4O_{11} slabs in the ε-SVO framework. Fig. 2b gathers the series of XRD diffractograms collected along the entire material discharge until Li_6SVO. For the latter material, the XRD analysis shows amorphous features except for the silver particles. The broadness of the reflections suggests nano-crystallinity of the extracted metallic silver. A crystallite size of *c.a.* 10 nm was estimated along the [1 1 1] by using the Debye-Scherrer formalism.

To gain further insight into SVO amorphization and Ag^0 extrusion, we integrated the area of the isolated (−3 1 2) diffraction peak of SVO ($2\theta = 32.19^\circ$) and the (1 1 1) of Ag^0. Their evolution as a function of the number of inserted lithium is reported in Fig. 3. Interestingly, neither silver metal nor signs of amorphization were detected below $x = 0.7$ Li^+ and ~0.55 Li^+, respectively; this indicates that the Ag^+/Li^+ displacement reaction is not initiated before this point.

Only beyond these thresholds is observed a linear amorphization of SVO until the electrode becomes XRD-amorphous at $Li_{2.2}Ag_2V_4O_{11}$. This particular composition is in good agreement with the observations reported by Leising et al. based on an *ex*

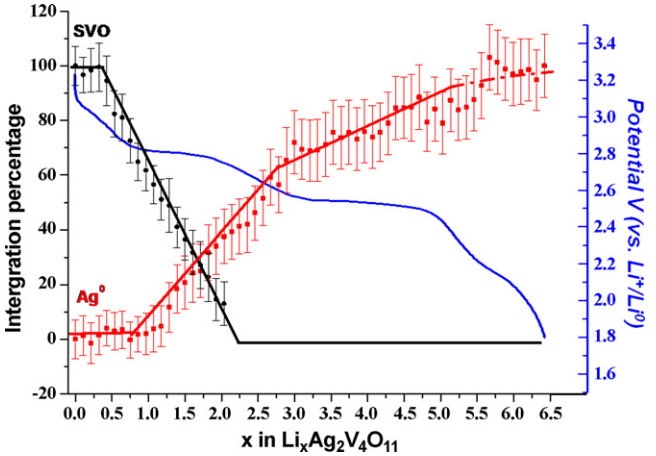

Fig. 3. Evolution of the silver metal and $Ag_2V_4O_{11}$ XRD diffraction peak area as a function of x in Li_x-SVO.

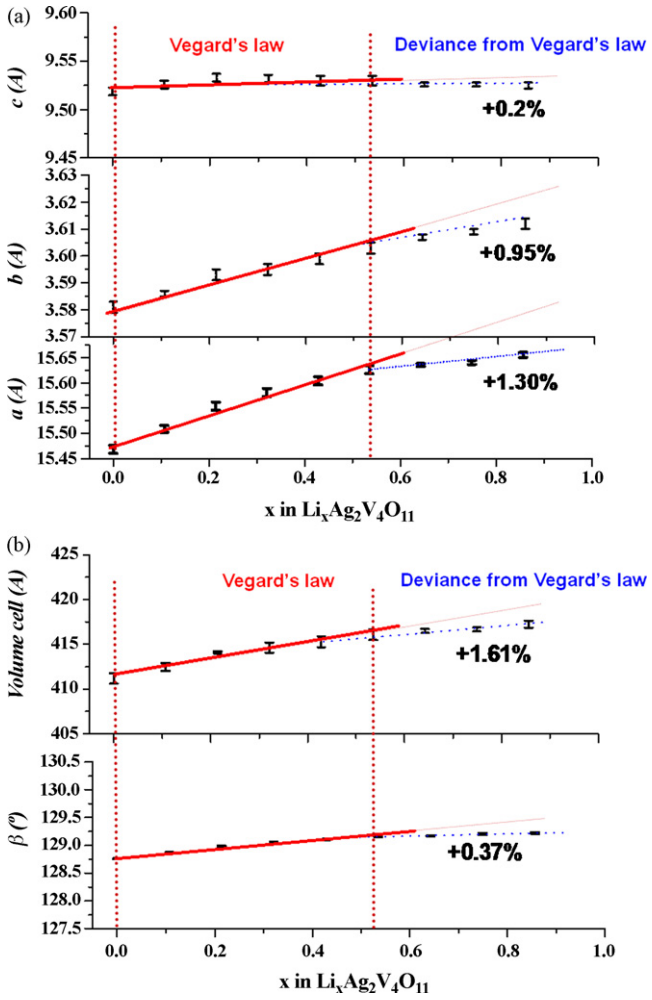

Fig. 4. Lattice cell parameter evolution as a function of x in Li_x-SVO for (a) a, b, c parameters and (b) β and cell volume.

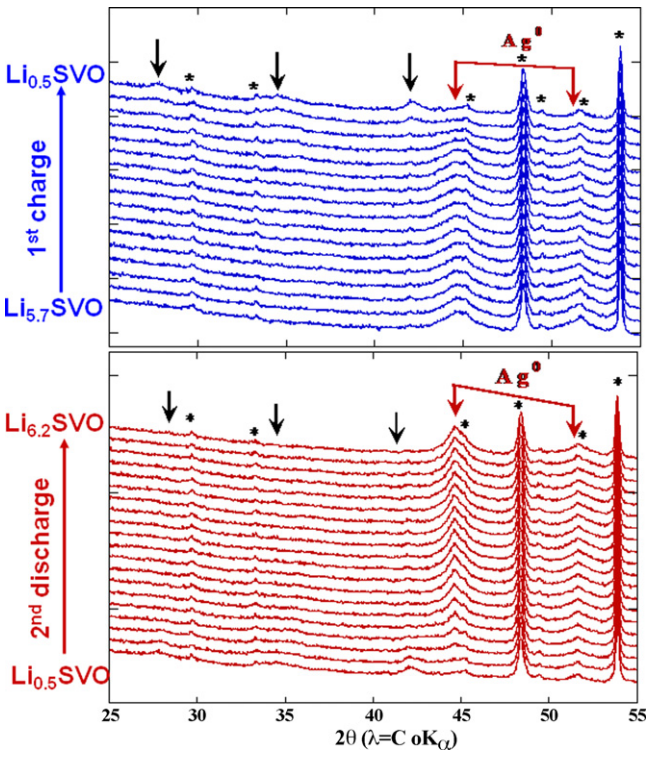

Fig. 5. *In situ* evolution of the XRD pattern during the 1st charge from $Li_{5.6}$-SVO to $Li_{0.4}$-SVO and the 2nd discharge from $Li_{0.4}$-SVO to $Li_{6.2}$-SVO.

situ XRD approach [3]. In contrast to the SVO amorphization, the changes in the silver metal are more complicated. We describe the evolution as the progression of two linear segments having a distinct slope that correlates with the feature of the first and second discharge plateaus. The reduction of silver ions mainly arises between $x \approx 0.7$ Li^+ and $x \approx 2.7$ Li^+. Although the crystallinity of the SVO particles is gone, the silver reduction proceeds throughout the second plateau. The fact that a slight intensity increase of the metallic silver peak area occurs after the second plateau does not rule out the hypothesis that a small amount of trapped silver ions can be still reducing at such low potentials.

Based on these results and our findings on two other silver oxyfluorides [20,21], a strong correlation exists between the amorphization of the vanadate structure and the silver extrusion.

The diffractograms collected for $x < 1$ were refined using Fullprof software in full-pattern matching mode and the evolution of the lattice cell parameters as a function of x lithium inserted is reported in Fig. 4 [22]. For $x < \sim 0.55$, the linear evolution between (a, b, c, β) as a function of the lithium content verifies Vegard's law. Beyond, a deviation from linearity is observed which originates from the onset of a competitive redox mechanism between the Ag^+/Li^+ displacement reaction and the reduction of V^{5+}. The [0 0 1] direction, which corresponds to the V_4O_{11} stacking planes, is only slightly influenced by the insertion of lithium with a $\Delta c/c$ expansion of only *c.a.* 0.2%. By contrast, the [1 0 0] and [0 1 0] directions show an increase of +0.95% and +1.30%, respectively (Fig. 4a). The β angle increases by +0.37% which yields an overall volume cell expansion of $\Delta V/V = 1.61\%$.

Because a displacement reaction and a conventional insertion reaction exhibit distinct electrochemical kinetics (*e.g.* $k^{\circ}_{(Ag^+)} \neq k^{\circ}_{(V5^+)}$ and $D_{(Li^+)} \neq D_{(Ag^+)}$), the reductive competition between Ag^+ and V^{5+} is expected to depend on the discharge rate while the silver displacement reaction is kinetically the slowest. This statement could explain the observation made by Leifer et al. showing that the silver reduction precedes the V^{5+} reduction in the specific circumstance where Li_xSVO samples were prepared at D/8760 (*i.e.* 1 Li^+ inserted per year) [15]. In this case, the existence of an internal redox process between V^{4+} and Ag^+ leading to $V^{5+} + Ag^0$ is neglected since ESR measurements on material freshly discharged and equilibrated in the battery for 4 months at $x = 1$ Li^+ did not show any modification in the V^{4+} content.

In addition to the first discharge, *in situ* XRD observations were also performed during the first recharge and on the second discharge. The V^{4+} is first oxidized followed by the uptake of Ag^+ as indicated by the progressive withdrawal of the silver metal diffraction peaks near the end of recharge (Fig. 5). It is worth noting that the silver re-injection (*i.e.* lithium de-insertion) does not induce re-crystallization into a highly ordered phase since the re-oxidized form remains structurally XRD-amorphous. Instead, the reversible appearance/disappearance of three very broad peaks is apparent (arrows in Fig. 5), which indicates a reversible structural reorganization restricted to the nano-scale. This is in contrast with the closely related copper vanadate $Cu_{2.33}V_4O_{11}$ where the re-injection of copper enables the original structure to be recovered [23]. This difference could be caused by the smaller ionic radius of copper, which prevents irreversible bending between V_4O_{11} slabs ($r_{(Cu+I)} = 0.77$ Å and $r_{(Cu+II)} = 0.73$ Å [19]).

The aforementioned potential difference, 300 mV for the first plateau (for $x < 3$ Li^+) and around 100 mV for the second, could thus be explained on the basis of this structural/environment modifi-

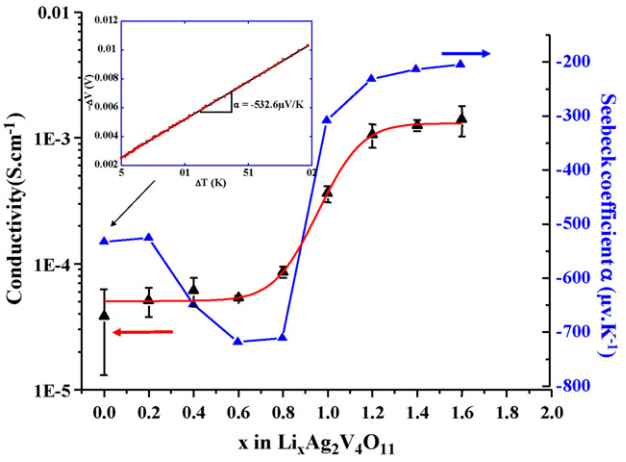

Fig. 6. *Ex situ* evolution of Li_x-SVO conductivity and Seebeck coefficient (α) as a function of the amount of lithium inserted (from $x = 0$ to $x = 1.6$) (in inset, example of a $-\Delta T = f(\Delta V)$ curve recorded for Li_0-SVO with the linear fit used for the Seebeck coefficient determination).

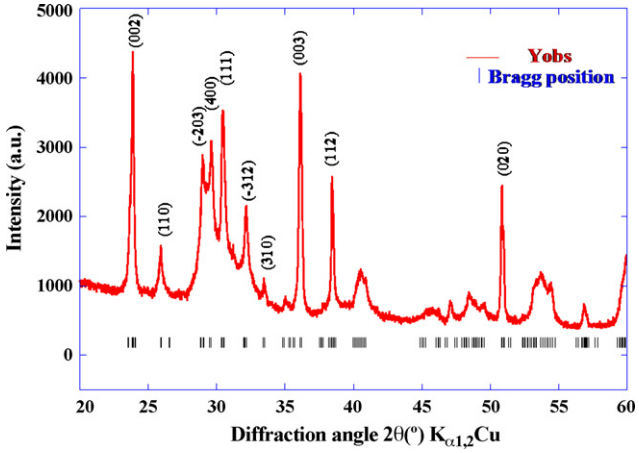

Fig. 7. XRD diffractogram of hydrothermal-synthesized SVO (SVO-HT).

cation between the first and second discharge and seems to most notably affect the electronic environment of Ag^+.

The evolution of the electrode transport properties as a function of the amount of lithium inserted was monitored by means of 4-probe DC conductivity and thermopower measurements. Initially, SVO-HT exhibits a room temperature conductivity of 3.8×10^{-5} S cm^{-1} ($\pm 2.5 \times 10^{-5}$ S cm^{-1}), which is about two orders of magnitude lower than that reported for solid-state reaction-made SVO products [2,24]. Meanwhile, the Seebeck coefficient was *c.a.* $-532.6\ \mu V\ K^{-1}$ and confirms n-type conduction in $Ag_2V_4O_{11}$ with an electron charge carrier density of $7.72 \times .10^{19}$ e$^-$ cm^{-3}. The low value of conductivity results from the intrinsically low mobility of the electrons within the structure, with $\mu = 3.071 \times 10^{-6}$ cm^2 V^{-1} s^{-1}. For $x < 0.6$, our result shows that the electrode conductivity is not affected. However, surprisingly, the reduction of V^{5+} gradually increase the electron mobility and decrease the charge carrier concentration in light of the Seebeck coefficient increases from $-532.6\ \mu V\ K^{-1}$ to $-718.1\ \mu V\ K^{-1}$ (Fig. 6). Between $0.6 < x < 1.2$, the conductivity is increased by two orders of magnitude from 5.35×10^{-5} S cm^{-1} ($\pm 0.21 \times 10^{-5}$ S cm^{-1}) to 1.06×10^{-3} S cm^{-1} ($\pm 0.22 \times 10^{-3}$ S cm^{-1}) as the result of the silver ion reduction which leads to nano-clusters of silver metal. This is accompanied by an increase in the charge carrier density to 2.28×10^{21} e$^-$ cm^{-3}, while the carrier mobility in Li_xSVO grains is maintained. Finally, although the reduction of silver metal still continues, the characteristics of conduction are not significantly modified beyond $x = 1.2$ Li^+. This is probably a result of the structural collapse.

Table 1
SVO-HT and SVO-SSR lattice cell parameters refined in pattern matching mode.

	a (Å)	*b* (Å)	*c* (Å)	*β*	Cell volume
SVO-HT	15.496(6)	3.589(2)	9.562(7)	128.67(2)	415.20(Å^3)
SVO-SSR	15.480(3)	3.582(1)	9.537(2)	128.74(1)	412.48(Å^3)

3.2. Electrochemical performances of hydrothermal-synthesized SVO

The recent synthetic investigation in the $Ag_2O/V_2O_5/HF_{(aq)}$ ternary system under hydrothermal conditions (150 °C) has enabled us to define a composition space where $Ag_2V_4O_{11}$ could be synthesized as a major phase [25]. After optimizing the synthetic procedure by adjusting the $Ag_2O/V_2O_5/HF_{(aq)}$ molar ratio, we produced $Ag_2V_4O_{11}$ as a single phase with a yield of 85% based on V (Fig. 7). The lattice cell parameters refined in full-pattern matching mode lead to values in good agreement with those refined on the SVO-SSR sample (see Table 1). The pristine SVO-HT particles exhibit a thin and flat needle-like morphology (Fig. 8) as is typically observed in the Ag/V/O system [26–31] and is similar to other hydrothermally made SVO [32,33]. The particle size varies between 2–5 μm in length and 0.21 μm in width for 50–100 nm in thickness.

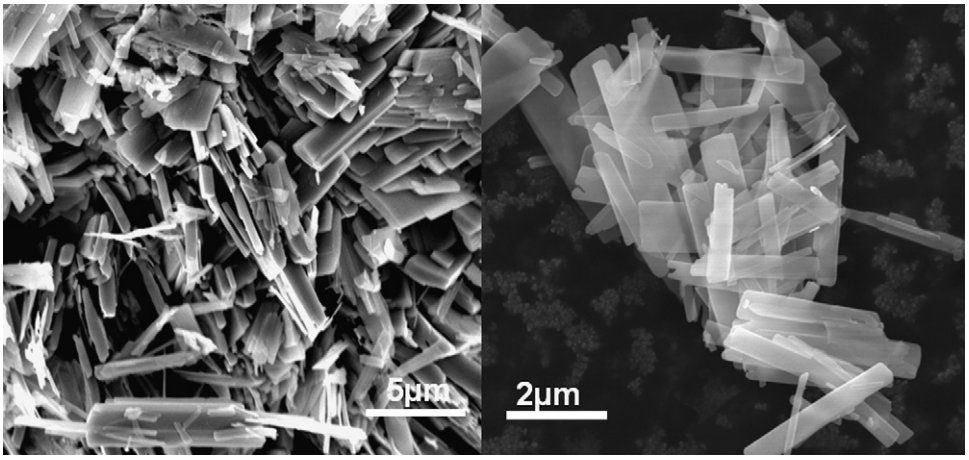

Fig. 8. Scanning electron micrographs of the pristine SVO-HT particles.

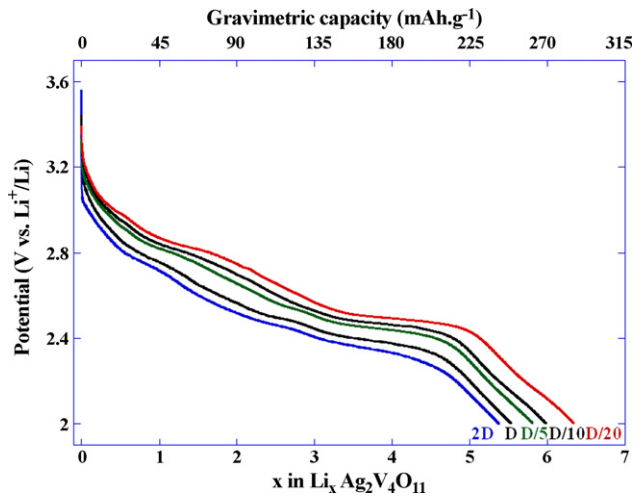

Fig. 9. Influence of the discharge rate on the SVO-HT capacity using a 1 M $LiPF_6$ EC/DMC 1:1 electrolyte.

The influence of the discharge rate on the electrode performance is reported in Fig. 9 where SVO-HT electrodes were discharged from D/20 to 2D (*i.e.* insertion of 1 Li^+ in 30 min). Interestingly, the increase in the discharge rate moderately influences the gravimetric capacity above 2 V (vs. Li^+/Li) since 286–245 mAh g^{-1} is recorded from D/20 to 2D. Such capacities favourably compare with those previously reported in the literature on SVO-SSR electrodes [3,5,6,8]. An identical electrochemical procedure and cell configuration was rigorously followed in order to compare the electrochemical properties of SVO-SSR and SVO-HT. The SVO-SSR particles ground with 14 wt.% C_{sp} produce rock-like fragments ranging from 10 μm to 50 μm. An increase in the particles' reactivity vs. lithium is experienced when using the SVO-HT product and more notably at high discharge rates leading to a higher gravimetric capacity above 2 V as well as a lowering in the electrode polarization as we recently also experienced in the case of SVOF prepared at room temperature that displays decreased particle size [34] (Fig. 10). This benefit in terms of reactivity vs. lithium is attributed to the 1D nano-sized character of the particles which permits a significant reduction in the Ag^+–Li^+/e^- path lengths in the solid. By this structural change, an 11% increase in the gravimetric capacity has been obtained at the 2D discharge rate (Fig. 10 inset).

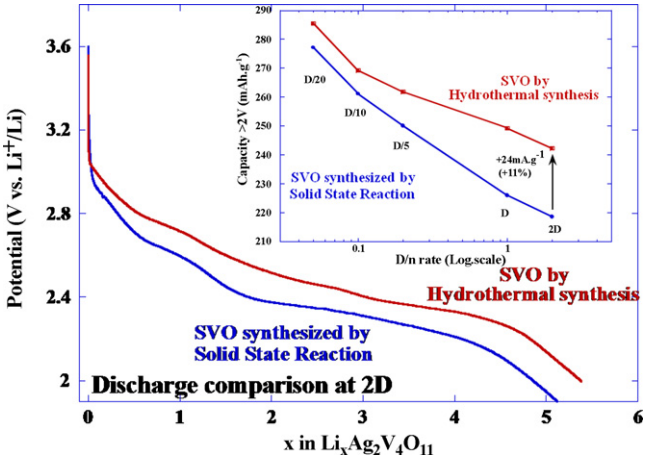

Fig. 10. Discharge curve comparison recorded at a 2D rate between $Ag_2V_4O_{11}$-SSR and $Ag_2V_4O_{11}$-HT materials. The evolution of the capacity recorded above 2 V (vs. Li^+/Li) as a function of discharge rate between $Ag_2V_4O_{11}$-SSR and $Ag_2V_4O_{11}$-HT particles is shown in inset.

4. Conclusion

In this work, we have combined *in situ* XRD, ESR, 4 probes DC conductivity and thermopower measurements to acquire a better understanding of the relationship between lithium content, electrode structure and transport properties. As a result, we pointed out the different stages of insertion as being (i) $0 < x < \sim 0.7$ a solid solution entailing the V^{5+} reduction without direct evidence of silver ions displacement, (ii) $\sim 0.7 < x < \sim 5.5$ Ag^+/Li^+ displacement reaction competing with V^{5+} reduction and (iii) $x > \sim 5.5$ reduction to $V^{4+} + \varepsilon$ of V^{3+}. The presence of the V^{5+}/V^{4+} couple does not significantly affect the electrode conductivity but the later formation of silver metal induces an increase of two orders of magnitude, from 3.81×10^{-5} S cm^{-1} to 1.41×10^{-3} S cm^{-1}. On the other hand, because of the significant ionic radii discrepancy between Ag^+ and Li^+, the displacement reaction causes the collapse of the structure, as shown by the amorphous character observed by PXRD from $Li_{2.2}Ag_2V_4O_{11}$. Interestingly, the electrochemically driven delithiation from $Li_6Ag_2V_4O_{11}$ did not allow the structure to re-crystallize to its original form although the silver ions re-entered the structure. Finally, beyond the scope of this fundamental investigation, we also reported superior electrochemical performances of hydrothermally made SVO particles using HF as a mineralizer. The smaller size of the particles, which exhibit a flat needle-like morphology with a thickness between 50 nm and 100 nm, noticeably increased particles' reactivity vs. lithium at high discharge rates. An 11% capacity gain above 2 V (vs. Li^+/Li) at a 2D discharge rate was experienced along with a decreased polarization.

Acknowledgements

The authors acknowledge Thomas A. Albrecht for fruitful discussions, Steve Harvey for his technical assistance with the thermopower equipments. This work was supported by the Office of Naval Research (MURI Grant N00014-07-1-0620). Vincent Bodenez is indebted to the Conseil Regional de Picardie (France) for financial support.

References

[1] K.J. Takeuchi, A.C. Marschilok, S.M. Davis, R.A. Leising, E.S. Takeushi, Coord. Chem. Rev. 219 (2001) 283–310.
[2] M. Onoda, K. Kanbe, J. Phys. Condens. Matter 13 (2001) 6675–6685.
[3] R.A. Leising, W.C. Thiebolt III, E.S. Takeuchi, Inorg. Chem. 33 (1994) 5733–5740.
[4] R.P. Ramasamy, C. Feger, T. Strange, B.N. Popov, J. Appl. Electrochem. 36 (2006) 487–497.
[5] J.W. Lee, B.N. Popov, J. Power Sources 161 (2006) 565–572.
[6] R.A. Leising, E.S. Takeuchi, Chem. Mater. 6 (1994) 489–495.
[7] S. Zhang, W. Li, C. Li, J. Chen, J. Phys. Chem. B 110 (2006) 24855–24863.
[8] S. Beninati, M. Fantuzzi, M. Mastragostino, F. Soavi, J. Power Sources 157 (2006) 483–487.
[9] K.J. Takeuchi, C.A. Marschilok, R.A. Leising, E.S. Takeuchi, MRS Symposium Proceedings, 2007, p. 972;
K.J. Takeuchi, C.A. Marschilok, R.A. Leising, E.S. Takeuchi, Solid State Ionics (2006) 351–356.
[10] R.A. Leising, E.S. Takeuchi, US Patent US2,003,138,697.
[11] E.S. Takeuchi, W.C. Thiebolt III, J. Electrochem. Soc. 135 (11) (1988) 2691–2694.
[12] K. West, A.M. Crespi, J. Power Sources 54 (1995) 334–337.
[13] N.R. Gleason, M. Palazzo, R.A. Leising, E.S. Takeuchi, K.J. Takeuchi, Abstract #248, in: 208th ECS Meeting, Los Angeles, USA, October, 2005.
[14] A.M. Crespi, P.M. Skarstad, H.W. Zandbergen, J. Power Sources 54 (1995) 68–71.
[15] N.D. Leifer, A. Colon, K. Martocci, S.G. Greenbaum, F.M. Alamgir, T.B. Reddy, N.R. Gleason, R.A. Leising, E.S. Takeuchi, J. Electrochem. Soc. 154 (6) (2007) A500–A506.
[16] D.S. McLachlan, M. Blaszkiewicz, R.E. Newnham, J. Am. Ceram. Soc. 73 (8) (1990) 2187–2202.
[17] H.L. Tuller, A.S. Nowick, J. Phys. Chem. Solids 38 (1977) 859–867.
[18] A.F. Ioffe, Physics of Semiconductors, Infosearch, London, 1960.
[19] R.D. Shannon, Acta Cryst. A32 (1976) 751.
[20] F. Sauvage, V. Bodenez, H. Vezin, T.A. Albrecht, J.-M. Tarascon, K.R. Poeppelmeier, Inorg. Chem. 47 (19) (2008) 8464–8472.
[21] F. Sauvage, V. Bodenez, J.-M. Tarascon, K.R. Poeppelmeier, submitted for publication.

[22] Fullprof (v. Dec. 2005), T. Roisnel (LCSIM, Rennes), J. Rodriguez-Carjaval (LLB, CEA-CNRS), France, 2005.
[23] M. Morcrette, P. Rozier, L. Dupont, E. Mugnier, L. Sannier, J. Galy, J.M. Tarascon, Nat. Mater. 2 (2003) 755–761.
[24] M.I. Bertoni, N.J. Kidner, T.O. Mason, T.A. Albrecht, E.M. Sorensen, K.R. Poeppelmeier, J. Electroceram. 18 (3–4) (2007) 189–195.
[25] T.A. Albrecht, C.L. Stern, K.R. Poeppelmeier, Inorg. Chem. 46 (2007) 1704–1708.
[26] M. Li, M. Shao, H. Ban, H. Wang, H. Gao, Solid State Ionics 178 (2007) 775–777.
[27] S. Kittaka, K. Matsuno, H. Akashi, J. Solid State Chem. 142 (1999) 360–367.
[28] S.J. Bao, Q.L. Bao, C.M. Li, T.P. Chen, C.Q. Sun, Z.L. Dong, Y. Gan, J. Zhang, Small Commun. 3 (7) (2007) 1174–1177.
[29] S. Kittaka, Y. Yata, K. Matsuno, H. Nishido, J. Mater. Sci. 35 (2000) 2185–2192.
[30] S. Kittaka, S. Nishida, T. Iwashita, T. Ohtani, J. Solid State Chem. 164 (2002) 144–149.
[31] P. Rozier, J. Galy, J. Solid State Chem. 134 (1997) 294–301.
[32] S. Shang, W. Li, C. Li, J. Chen, J. Phys. Chem. B 110 (2006) 24855–24863.
[33] K.J. Takeuchi, A.C. Marschilok, R.A. Leising, E.S. Takeuchi, Mater. Res. Soc. Symp. Proc. 972 (2007) 351–356.
[34] T.A. Albrecht, F. Sauvage, V. Bodenez, J.-M. Tarascon, K.R. Poeppelmeier, Chem. Mater. 21 (13) (2009) 2017–2020.